Design of DGT-based Linear and Non-Linear Equalizers for GFDM Transmission

Francesco Linsalata[a], Atul Kumar[b], Maurizio Magarini[a]

[a] *Dipartimento di Elettronica, Informazione e Bioingegneria, Politecnico di Milano, Italy, (email: name.surname@polimi.it)*
[b] *Vodafone Chair Mobile Communications Systems, Technische Universität Dresden, Germany (email: atul.kumar@tu-dresden.de)*

Abstract

This paper exploits the parallelism between Discrete Gabor Transform (DGT) and Generalized Frequency-Division Multiplexing (GFDM) that exists when the synthesis function, i.e. the pulse shaping filter, and the analysis function, i.e. the receiving filter, satisfy the Wexler-Raz identity. Choosing functions that satisfy the Wexler-Raz condition allows optimal symbol-by-symbol detection for a DGT-based GFDM receiver in case of transmission over an additive white Gaussian noise channel. However, multipath fading is the major problem of the wireless communication channel, hence, when transmission takes place over frequency selective channel, symbol-by-symbol detection is no longer optimal due to interference generated among the transmitted symbols. In this work, we deal with the design of linear and non-linear receivers for DGT-based GFDM transmission over a frequency selective channel that allows a good trade-off between complexity and performance. Different equalization schemes to mitigate distortions, such as Maximum Likelihood, Zero-Forcing and Minimum Mean-Squared Error, are developed and analyzed. Monte Carlo simulations are used to evaluate the error rate performance achieved with the considered design. A comparison is done with other works in the literature.

Discrete Gabor transform (DGT), Maximum-Likelihood detection, linear equalization, generalized frequency division multiplexing (GFDM).

⋆A preliminary version of the work was presented in Balkancom '19.

1. Introduction

In the recent years, intensive successful testing, proof-of-concepts and trials have supported the launch of the fifth generation (5G) cellular networks. The development of 5G introduces a new paradigm. In fact, it is expected to be based on complete wireless communications without limitations [1], i.e. the new technology will be available for each user experience and each part of the access network. Thus, a lot of challenges will influence the design of communication networks and many open-ended research opportunities [1, 2].

In particular, 5G will provide: enhanced Mobile Broadband communication (eMBB), Ultra-Reliable Low-Latency Communications (URLLC), and Machine Type Communications (MTC) [4, 3]. Among these, eMBB is expected to allow theoretical user throughputs up to 10 Gbps in uplink and up to 20 Gbps in downlink by adopting technologies such as multi band carrier aggregation, enhanced channel modulation schemes, massive Multiple-Input/Multiple-Output (MIMO), and licensed assisted access [1]; URLLC imply reduction of the time taken by a packet to go from the transmitter to the receiver with a low probability of error; MTC is an innovative form of data communication which involves one, or more, entities that do not necessarily need human interaction.

On the other hand, the concept of network slicing, which uses resources when, and where, needed and then releases them, will play a critical role in 5G networks because of the very wide gamut of expected use cases and services. Extending slicing to physical layer is still an open issue [2].

These new 5G benefits will allow for a more "connected world", i.e. a single platform that enables a variety of different services, animated driving, Industry 4.0, Internet-of-Everything (smart home appliances) [1] [2].

To address the above challenges at the physical layer, the concept of Software Defined Artificial Intelligence and Air Interface (SD-AI^2) has been recently proposed with the aim to dynamically adapt the numerology of one link based on the user environment [2] . To enable SD-AI^2, link adaptation mechanisms for several fundamental building blocks, such as waveform, frame structure,

multiple access scheme, modulation and coding, etc. need to be well designed [2].

A key requirement in the physical layer of future cellular networks is the flexibility to support mixed services with different waveform parameters within one carrier [5, 6, 7, 8]. From the perspective of waveforms design, many new solutions have been investigated. These need to be characterized by very high spectral efficiency, relaxed synchronization, low out-of-band (OOB) emission [3] and, additionally, to be able to support variable and customizable pulse shaping filters, achieving a better trade-off between time-domain and frequency-domain localization [4, 3].

Among the most discussed waveforms, there are Orthogonal Frequency-Division Multiplexing (OFDM) and Generalized Frequency Division Multiplexing (GFDM). Both of them are based on a Frequency-Division Multiplexing (FDM) approach where signals are transmitted in parallel using different subcarriers. The two proposed systems are very similar but with different advantages and disadvantages. Since pros and cons of OFDM are well known, in what follows we will focus on GFDM. In particular, GFDM exploits both frequency and time domain for symbols transmission and relies on traditional filter bank multicarrier concept and on circular filtering at sub-carrier level [9, 10]. Compared to OFDM, the main advantages of GFDM consist in a reduction of the OOB emission [7], and in an increase of the spectral efficiency, obtained through the introduction of tail biting, which makes the length of the cyclic prefix (CP) independent from that of pulse shaping filter [11, 12]. The low latency and malleability requirements, which are the major challenges in the tactile Internet scenario, can be fulfilled by GFDM due its flexible block structure, which allows to cover both CP-OFDM and single carrier transmission, such as Single Carrier FDM (SC-FDM) or DFT-spread-OFDM [11].

The high peak-to-average power ratio (PAPR) of the OFDM is a very well known limitation and can impede good downlink and uplink performance [13, 14]. In contrast, the additional degree of freedoms from the adjustable subcarrier filters in GFDM allow further control of the PAPR [15] and, moreover,

several advantages of GFDM have been already brought to MIMO application without increasing the system complexity [16].

However, these GFDM performance gains come at the cost of non-orthogonal (or semi-orthogonal) transmission, which leads to an increase of Bit Error Rate (BER) and requires a more complex receiver. In fact, when it comes to complexity comparison, GFDM requires higher complexity than OFDM. The main issue of GFDM compared to OFDM is the need of equalization, implemented by block-based processing in time or frequency domain, which is required even in the case of transmission over an ideal channel [10, 17].

For an efficient implementation of the GFDM receiver in time-domain, a relationship between GFDM and discrete Gabor transform (DGT) was proposed in [18]. It was shown that GFDM transmission and reception are equivalent to a finite discrete Gabor expansion and DGT in critical sampling, respectively. The author of [18] provided an efficient algorithm for calculation of specific GFDM receiver filters in time domain for non-frequency selective channel. An equivalent interpretation of the DGT receiver in frequency-domain was given in [19], which allows for signal recovery with lower complexity compared to the time-domain approaches. It is worth observing that when transmission over a frequency-selective channel is considered the DGT interpretation with critical sampling loses its validity. In this case, to restore the condition required for using DGT at the receiver, the effect of the channel must be taken into account in the equalization of the whole GFDM symbol. This aspect was considered in [19], where it was observed that the performance of the proposed low complexity frequency-domain equalization approach for the DGT-based GFDM system was close to that of OFDM only when the number of sub-symbols transmitted on each sub-carrier is low. When this number increases a rapid degradation in the performance is observed due to the inter-sub-symbol interference (ISSI) among the sub-symbols transmitted on the same sub-carrier [20], which is not properly considered in [19]. Thanks to this novel concept, we investigate the possibility to use the domain time approach of [18], which takes into account the frequency selectivity of the channel, to achieve a good trade-off between error

rate and complexity. Moreover, the use of the Dirichlet function, here proposed, allows the DGT based GFDM system to reach the lower-bound of the theoretical performance in case of non-frequency selective channels, which is an aspect not discussed in [18, 19]. Furthermore, the main contribution of this paper consists in the use of a mathematical model for the received signal to design time-domain equalizers that combat ISSI on a sub-carrier basis. This makes possible to evaluate the best strategy for detecting the transmitted symbols according to the desired performance and degree of complexity. In particular, we will focus on the design of linear equalization schemes, such as Zero-Forcing (ZF), Minimum Mean-Squared Error (MMSE) and Matched Filter (MF) and we will compare their performance and complexity with respect to the optimal non-linear Maximum Likelihood Detection (MLD). Instead, in case of a multi-path frequency selective channel, the superior performance achieved by different equalization approaches that exploit the proposed modelling will be shown with respect the other solutions present in the literature that do not take into account such a knowledge. The proposed GFDM design can also be beneficial to develop future non-linear and recursive detection algorithms.

The structure of the paper is as follows. In Sec. 2 we will introduce the DGT interpretation of GFDM while the results in case of transmission over a non-frequency selective channel are shown in Sec. 3. The mathematical model in case of transmission over frequency selective channels is reported in sec. 4. The design of the different types of receivers will be considered and discussed in Sec. 5. Section 6 will present the results of Monte Carlo simulations and Sec. 7 analyzes the complexity of the proposed receivers. Finally, conclusion will be drawn in Sec. 8.

2. DGT-based GFDM System Model

Dennis Gabor introduced in 1946 in his "Theory of Communication" a method to represent a signal as a linear combination of time and frequency coordinates. According to the given representation, each coordinate is well con-

centrated in time and frequency domain. Therefore, it is possible to define a complete collection of building blocks to decompose complicated signals. Yet, despite the long history of the Gabor framework and a lot of work by mathematicians, physicists and engineers alike, there are still many interesting and useful aspects of the Gabor transform to be explored and exploited [21]. In fact, a parallelism with the GFDM modulator and demodulator was shown in [18] and it is here illustrated. With reference to one GFDM symbol, the block of transmitted bits is applied to the input of a mapper that gives at its output an $M \times K$ data matrix $\mathbf{X}$ whose $N = MK$ elements take values from a complex constellation, *e.g.*, phase-shift keying [12]. The data matrix $\mathbf{X}$ is sent to the GFDM modulator, based on K sub-carriers, where each sub-carrier is used to transmit M sub-symbols. According to this model the data matrix $\mathbf{X}$ can be represented as the composition of K column vectors

$$\mathbf{X} = [\mathbf{X}_0, \mathbf{X}_1, \cdots, \mathbf{X}_{K-1}], \tag{1}$$

where

$$\mathbf{X}_q = [X_q(0), X_q(1), \cdots, X_q(M-1)]^T, \tag{2}$$

with $X_q(m)$ representing the mth sub-symbol, $m = 0, \ldots, M-1$, transmitted on the qth sub-carrier, $q = 0, \ldots, K-1$ and $(\cdot)^T$ denoting the transposition operation. The time-duration of each symbol vector $\mathbf{X}_q$ is MT_s with sub-carrier spacing equal to $1/(MT_s)$, T_s being the symbol interval on each sub-carrier. The M sub-symbols of the kth group are upsampled by a factor K and applied to the input of a periodic pulse shaping filter with N coefficients. After pulse shape filtering, the nth sample of the transmitted GFDM signal is written as:

$$\begin{aligned} x(n) &= \sum_{q=0}^{K-1} \sum_{m=0}^{M-1} X_q(m) g_{q,m}[n] \\ &= \sum_{q=0}^{K-1} \sum_{m=0}^{M-1} X_q(m) g[\langle n - mK \rangle_N] \, e^{\frac{j2\pi qn}{K}}, \end{aligned} \tag{3}$$

where $n = 0, 1, \cdots, N-1$, is the sampling index and $\langle \cdot \rangle_N$ denotes the modulo N operation that implements the circular shifting of the periodic prototype

discrete-time impulse response $g\,[n]$ of length N. As first observed in [18], equation (3) can be interpreted as an inverse DGT (IDGT), where $g[n]$ represents the synthesis function whose time-domain translations and frequency-domain shiftings $g_{q,m}[n]$ are weighted by transmitted symbols. With this interpretation, in case of transmission over an ideal channel the symbols $X_q(m)$ can be recovered from $x(n)$ at the receiver by applying the DGT as

$$X_q(m) = \sum_{n=0}^{N-1} \gamma^*_{q,m}[n] x(n), \tag{4}$$

where $\gamma_{q,m}$ is a periodic discrete function with period N, which is defined as the analysis function obtained from time and frequency shifts of an discrete-time window $\gamma[n]$ and can be written as:

$$\gamma_{q,m}[n] = \gamma\left[\langle n - mK\rangle_N\right] e^{\frac{j2\pi qn}{K}}. \tag{5}$$

Note that, the identity defined by (4) holds only when the synthesis function $g[n]$ and the analysis function $\gamma[n]$ satisfy the *Wexler-Raz* identity given in [19, eq. (11)]. If this condition is not satisfied interference arises both from symbols transmitted on other sub-carriers and from sub-symbols transmitted on the same sub-carrier. As a function satisfying the Wexler-Raz identity with critical sampling in what follows we consider a Dirichlet pulse, also referred *discrete sinc*, which is characterized by a DFT that is a rectangular pulse, and can be written as

$$G_q^D = \begin{cases} 1, & \left(0 \le q \le \lceil \frac{M}{2} \rceil - 1\right) \bigcup \left(N - \lfloor \frac{M}{2} \rfloor \le q \le N-1\right), \\ 0 & otherwise, \end{cases} \tag{6}$$

where $\lceil \cdot \rceil$ and $\lfloor \cdot \rfloor$ denote the nearest upper and lower integer, respectively. With the use of Dirichlet function we have $\gamma[n] = g[n]$, and the filtering implemented at the receiver with the analysis function $\gamma[n]$ can be therefore interpreted as satisfying the matched and ZF condition at the same time.

3. Transmission over Non-Frequency Selective Channels

The Additive White Gaussian Noise (AWGN) model describes a channel whose effect consists in the addition of a white Gaussian noise process to the

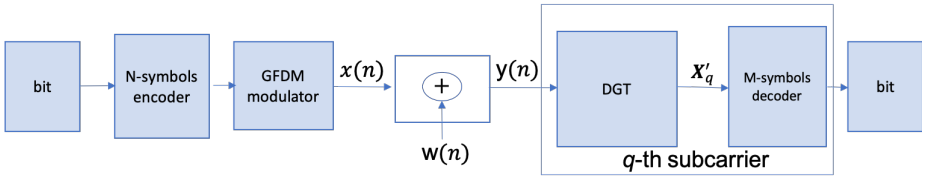

Figure 1: DGT-based GFDM transmitter and receiver block diagram in case of an AWGN channel.

transmitted signal, as shown in Fig.. 1.

The channel is mathematically described by

$$y(n) = x(n) + w(n), \quad n = 0, 1, \ldots, N-1, \tag{7}$$

where the nth sample $y(n)$ of the received signal is given by the sum of the transmitted signal $x(n)$ and a zero-mean complex white Gaussian process $w(n)$ with variance N_0. The receiver performs the DGT, as in (4), for each m, q pairs as:

$$X'_q(m) = \sum_{n=0}^{N-1} \gamma^*_{q,m}[n] y(n). \tag{8}$$

Then, the sequence of symbols $X'_q(m)$ is sent to the decoder. The decoder makes the optimal decision about which message is transmitted. An optimal decision means a decision rule that minimizes the probability of error between the transmitted message $X_q(m)$ and $X'_q(m)$. The BER performance, in case of QPSK modulation with M=5 and K=32, is reported in Fig. 2 as function of the Signal-to-Noise Ratio (SNR) per bit, which is defined as the ratio E_b/N_0 between the energy associated to each bit and the noise variance.

In the same plot the theoretical BER performance is reported for the considered modulation schemes. As can be observed, the Dirichlet pulse makes the DGT based GFDM system orthogonal reaching the theoretical BER for the used modulation, as OFDM in an AWGN channel. GFDM with Dirichlet pulse can therefore be regarded as a "reversed OFDM" where the rectangular pulse shaping is applied in the frequency domain instead of the time domain.

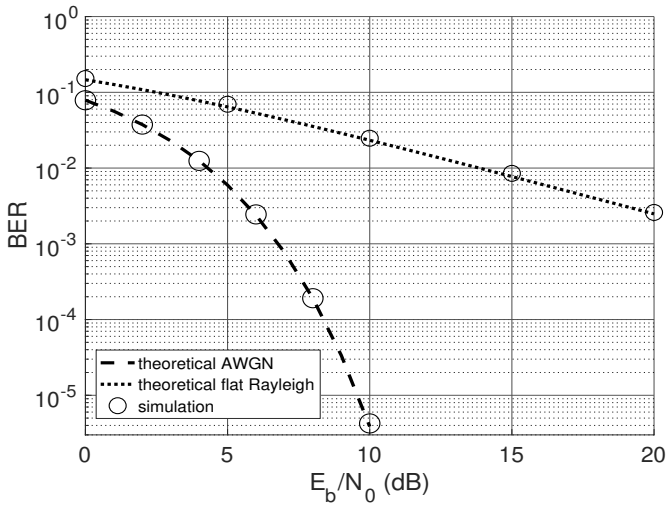

Figure 2: BER vs. E_b/N_0 for DGT-based GFDM in case of QPSK transmission over an AWGN and flat Rayleigh channel for M=5 and K=32.

We also report in Fig. 2 the Monte Carlo simulations and theoretical results of the BER versus SNR per bit for GFDM transmission when QPSK symbols are transmitted over a flat Rayleigh fading channel. This channel is modelled as:

$$h\left(t\right) = h_0 \delta\left(t\right), \tag{9}$$

where h_0 is a Rayleigh distributed random variable, which is considered as a constant parameter for the entire duration of the GFDM symbol transmission [23]. From these results, it is evident that GFDM based on DGT interpretation has the same theoretical performance as that of QPSK in case of transmission over non-frequency selective channels.

4. Transmission over Frequency-selective Channels

When transmission takes place over a classical wireless channel, i.e. characterized by delay spread and fading effect, different types of interference arise, requiring a higher complexity for the GFDM demodulation procedure with re-

spect to the OFDM case. This is one of the main motivations behind this work. In fact, low complexity solutions must be looked for to reduce the complexity of the system and that are suitable for hardware implementation at the same time.

As in the case of OFDM, the main impairments for GFDM are Inter Carrier Interference (ICI), which introduces a loss of orthogonality between symbols transmitted on different sub-carriers and Inter Symbol Interference (ISI), which is due to the time-dispersion of the channel. The effect of ISI can be mitigated by inserting a CP, which consists of N_{CP} samples such that the length of the CP is at least equal to the length of the channel. The CP-extended signal is written as

$$\tilde{x}(n) = \begin{cases} x(N+n), & n = -N_{CP}, \ldots, -1, \\ x(n), & n = 0, \ldots, N-1. \end{cases} \tag{10}$$

It is important to underline that for a GFDM signal only one CP is needed for the entire packet transmission, i.e. N symbols. In contrast, for the OFDM case, one CP is required for each OFDM packet, i.e. K. However, the GFDM signal spans among K sub-carriers $N = MK$ symbols, instead only K symbols in case of OFDM scheme are transmitted, leading to an increase of the overall system spectral efficiency [22]. This means an GFDM gain, proportional to M in terms of the overall spectral efficiency with respect to the OFDM case [22].

The same L-path tapped delay line channel model defined in [23] is considered. According to this model, the continuous-time impulse response of the multi-path fading channel is defined as

$$h(t) = \sum_{i=0}^{L-1} h_i \delta(t - \tau_i), \tag{11}$$

where h_i is the complex amplitude, *i.e.*, tap coefficient, of the ith path associated with the propagation delay τ_i and $\delta(t)$ is the delta Dirac function. In the following, for simplicity, we consider the case where $\tau_i = i$, with $i = 0, \ldots, L-1$. The tap coefficients h_i, $i = 0, 1, 2, \ldots, L-1$, are modeled as independent and identically distributed zero mean complex random variables with average

power $\sigma_i^2 = 1/L$, uniform distributed phase in $[0, 2\pi)$, and Rayleigh distributed amplitude. According to such a model we have $\sigma_0^2 + \sigma_1^2 + \cdots + \sigma_{L-1}^2 = 1$. Note that, when $L = 1$ we get the flat fading Rayleigh channel model (9). For the particular case where h_0 is constant and equal to 1 we have the ideal channel.

After passing through the channel the received signal is written as

$$y(n) = \sum_{i=0}^{L-1} h_i \tilde{x}(n-i) + w(n), \tag{12}$$

where $w(n)$ represents the complex AWGN with zero mean and variance N_0 per dimension. Under the assumption $N_{CP} \geq L-1$, by removing the effect of the cyclic prefix and by replacing (3) in (12) we get

$$y(n) = \sum_{i=0}^{L-1} h_i \sum_{q=0}^{K-1} \sum_{m=0}^{M-1} X_q(m) g[\langle n-i-mK \rangle_N] \, e^{\frac{j2\pi q(n-i)}{K}} + w(n). \tag{13}$$

In order to recover the transmitted symbols, the DGT defined in (4) is applied to the received signal as

$$\begin{aligned} Y_q(m) &= \sum_{n=0}^{N-1} \gamma_{q,m}^*[n] y(n) = \sum_{n=0}^{N-1} \gamma^*[\langle n - mK \rangle_N] \, y(n) \, e^{-\frac{j2\pi qn}{K}} \\ &= \sum_{k=0}^{K-1} \sum_{l=0}^{M-1} X_k(l) \sum_{i=0}^{L-1} h_i \underbrace{\left\{ \sum_{n=0}^{N-1} \gamma^*[n] g[\langle n-i+(m-l)K \rangle_N] e^{\frac{-j2\pi(q-k)n}{K}} \right\}}_{P_k[l,i]} e^{\frac{-j2\pi ki}{K}} \\ &\quad + W_q(m), \end{aligned} \tag{14}$$

where $W_q(m)$ is the DGT of the AWGN and

$$\begin{aligned} P_{kM}[l,i] &= \sum_{n=0}^{N-1} \gamma^*[n] \, g[\langle n - i + lK \rangle_N] \, e^{-\frac{j2\pi kn}{K}} \\ &= \frac{1}{N} \sum_{q=0}^{N-1} \Gamma_q^* G_{\langle q+kM \rangle_N} e^{-\frac{j2\pi(q+kM)(i-lK)}{N}} \\ &= \left(\frac{1}{N} \sum_{q=0}^{N-1} \Gamma_q^* G_{\langle q+kM \rangle_N} e^{\frac{j2\pi ql}{M}} e^{-\frac{j2\pi qi}{N}} \right) e^{-\frac{j2\pi ki}{K}} \end{aligned} \tag{15}$$

with Γ_q and G_q corresponding to the N-points DFT of $\gamma[n]$ and $g[n]$, respec-

tively. By setting $G_k = G_k^D$ in (15) we get

$$P_{kM}[l,i] = \left(\frac{1}{N}\sum_{q=0}^{N-1}\Gamma_q^* G_{\langle q+kM\rangle_N} e^{\frac{j2\pi ql}{M}} e^{-\frac{j2\pi qi}{N}}\right) e^{-\frac{j2\pi ki}{K}}$$
$$= \begin{cases} \delta[k]\frac{1}{N}\sum_{q=-(M-1)/2}^{(M-1)/2} e^{-\frac{j2\pi q(i-lK)}{N}} = \delta[k]\frac{1}{N}\frac{\sin(\frac{\pi(i-lK)}{K})}{\sin(\frac{\pi(i-lK)}{N})}, M \text{ odd} \\ \delta[k]\frac{1}{N}\sum_{q=-M/2}^{M/2-1} e^{-\frac{j2\pi q(i-lK)}{N}} = \delta[k]\frac{1}{N}\frac{\sin(\frac{\pi(i-lK)}{K})}{\sin(\frac{\pi(i-lK)}{N})} e^{\frac{j\pi(i-lK)}{N}}, M \text{ even} \end{cases} \quad (16)$$

where $\delta[k]$ denotes the Kronecher delta. In the special case $i = 0$, eq. (15) converted into eq. (14) of [19] for which we obtain the Wexler-Raz identity

$$P_{kM}[l,0] = \sum_{n=0}^{N-1}\gamma_{k,m}^*[n]\, g\left[\langle n+lK\rangle_N\right] e^{-\frac{j2\pi kn}{K}}$$
$$= \frac{1}{N}\sum_{q=0}^{N-1}\Gamma_q^* G_{\langle q+kM\rangle_N} e^{\frac{j2\pi ql}{M}} = \delta_k\delta_l, \quad (17)$$

By substituting $P_{kM}[lK,i]$ given in (16) into (14) and after some mathematical manipulation (14) can we rewritten as

$$Y_q(m) = \sum_{l=0}^{M-1} X_q(l) \sum_{i=0}^{L-1} h_i \frac{\sin\left(\frac{\pi(i-(m-l)K)}{K}\right)}{\sin\left(\frac{\pi(i-(m-l)K)}{N}\right)} e^{\frac{-j2\pi qi}{K}} + W_q(m)$$
$$= \sum_{l=0}^{M-1} X_q(l)\bar{H}_{qM}\left((m-l)K\right) + W_q(m), \quad (18)$$

where the even property of the periodic Dirichlet sinc function has been used. The above equation shows that in case of Dirichlet function the interference is generated only by sub-symbols transmitted on the same sub-carrier and not from sub-symbols transmitted on other sub-carriers. The "windowed" channel is given by

$$\bar{H}_q(m) = \sum_{i=0}^{N-1} h_i^{(ZP)} w_{\langle i-m\rangle_N} e^{\frac{-j2\pi qi}{N}}, \quad (19)$$

where $w_{\langle i-m\rangle_N}$ corresponds to a shifting of m samples of the periodic windowing function

$$w_n = \frac{\sin\left(\frac{\pi n}{K}\right)}{\sin\left(\frac{\pi n}{N}\right)}, \qquad n = 0,\ldots,N-1, \quad (20)$$

and

$$h_i^{(ZP)} = \begin{cases} h_i & i = 0, \ldots, L-1, \\ 0 & i = L, \ldots, N-1. \end{cases} \tag{21}$$

Equation (19) can be rewritten as

$$\bar{H}_q(m) = H_q \otimes_N W_q e^{-j\frac{2\pi mq}{N}}, \tag{22}$$

which is the circular convolution between the DFT of the channel and the DFT of the shifted windowing function, where $W_q = G_q^D$. According to the definition of G_k^D given in (6), eq. (22) realizes a weighted average of M frequency domain values of H_k around $k = q$, where the weights are obtained from the complex exponential for a given m. The M samples H_k involved in the average are $k = \langle q - \lfloor \frac{M}{2} \rfloor, \ldots, q-1 \rangle_N$ and $k = \langle q, \ldots, q + \lceil \frac{M}{2} \rceil - 1 \rangle_N$, which define the M points around q taking into account of the periodic nature of H_k. Equation (18) can be rearranged as

$$Y_q(m) = X_q(m)\bar{H}_{qM}(0) + \sum_{l=0, l\neq m}^{M-1} X_q(l)\bar{H}_{qM}((m-l)K) + W_q(m), \tag{23}$$

where it appears that the mth sub-symbol transmitted on the qth sub-carrier $X_q(m)$ is

- scaled by the term $\bar{H}_{qM}(0)$;
- impaired by the interference generated by the mth sub-symbol transmitted on the same sub-carrier through the term $\bar{H}_{qM}(m-l)K$, $l \neq m$;
- distorted by the AWGN term $W_q(m)$.

5. Design of Linear and Non-Linear Receivers

With reference to (24), we define the vector of the received signal $\mathbf{Y}_q = [Y_q(0), Y_q(1), \ldots, Y_q(M-1)]^T$ on the qth sub-carrier, which is given by

$$\mathbf{Y}_q = \bar{\mathbf{H}}_{qM}\mathbf{X}_q + \mathbf{W}_q, \qquad q = 1, \ldots, K-1, \tag{24}$$

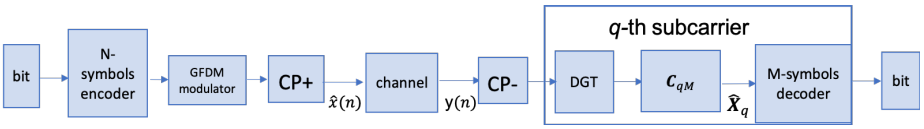

Figure 3: GFDM transmitter and receiver block diagram with per sub-carrier linear detection.

where $\mathbf{W}_q = [W_q(0), W_q(1), \ldots, W_q(M-1)]^T$ and

$$\bar{\mathbf{H}}_{qM} = \begin{bmatrix} \bar{H}_{qM}(0) & \bar{H}_{qM}(N-K) & \cdots & \bar{H}_{qM}(N-(M-1)K) \\ \bar{H}_{qM}(N-(M-1)K) & \bar{H}_{qM}(0) & \cdots & \bar{H}_{qM}(N-K) \\ \vdots & \vdots & \ddots & \vdots \\ \bar{H}_{qM}(N-K) & \bar{H}_{qM}(N-2K) & \cdots & \bar{H}_{qM}(0) \end{bmatrix}. \tag{25}$$

It is worth noting that the model in (24) is the same as that used to describe the received vector in a MIMO system [26]. With this interpretation it is possible to design several types of receivers according to the desired trade-off between performance and complexity.

The optimal scheme, in the sense of minimization of the error probability, is the MLD approach. For small numbers of transmit antennas (or symbols per sub-carrier in the considered case) and low-order constellations (BPSK, QPSK, 4-QAM) the complexity of MLD is not overwhelming. The estimated symbol vector is:

$$\hat{\mathbf{X}}_q = \arg \min_{\mathbf{X} \in \mathcal{X}^M} \left\| \mathbf{Y}_q - \bar{\mathbf{H}}_{qM} \mathbf{X} \right\|^2, \tag{26}$$

where $\|\cdot\|$ denotes the norm and $\mathbf{X}$ is the vector of input symbols taken from the M-dimensional space $\mathcal{X}^M$, with $\mathcal{X}$ being the alphabet of the used constellation. With MLD, the optimal performance is achieved by means of an exhaustive search over all the combinations of symbols. Although the complexity of MLD is quite high, being it proportional to $\mathcal{X}^M$, it can be considered as a reference against which to compare the performance of any sub-optimal ones [24].

However, low complexity, yet high-performance, sub-optimal detection algorithms can be proposed in practical applications [25]. Hence, with reference to

the scheme defined in Fig. 3, we here consider the use of per sub-carrier linear receivers to estimate the transmitted symbols. In general, linear receivers are known for their appealingly low complexity, but suffer from a considerable performance loss in comparison to MLD [25]. This class of detectors linearly combine the received signals to form an estimate of the transmitted symbols. The linear combination can be represented in matrix form as:

$$\hat{\mathbf{X}}_q = \mathbf{C}_{qM}\mathbf{Y}_q. \tag{27}$$

Then, a threshold detector is used to decide independently the M symbols. The linear weighting matrix $\mathbf{C}_{qM}$ can be designed both by using different criteria [25]. The details of each receiver are describe below:

- **MF Receiver** is the lowest complexity receiver [28] among all practical MIMO detectors and its weight matrix is expressed as:

  $$\mathbf{C}_{qM,\mathrm{MF}} = \bar{\mathbf{H}}_{qM}^{H} \tag{28}$$

  where ^{H} denotes Hermitian transpose conjugation. The main problem of such a type of receiver is related to interference mitigation. In fact, it is not able to reduce the interference of the other $M-1$ symbols transmitted on the same sub-carrier and it leads to irreducible error floor even if in the case of SNR that tends to infinite. On the other hand, if the co-channel interference is negligible, then the MF detector may perform similar to the optimal detector since the MF maximizes the output SNR. Linear MF equalization was widely used before the concept of MIMO detection was born and it is essentially based on the single user detection philosophy. Hence, it does not belong to the joint detection-based MIMO detection family, and typically it exhibits a poor performance. In the low SNR region, the performance of linear MF detector is expected to be similar to that of MLD [25] [28];

- **ZF Receiver** applies the inverse of the channel frequency response to the

received signal, to restore the signal after the channel

$$\mathbf{C}_{qM,\mathrm{ZF}} = (\bar{\mathbf{H}}_{qM}^{H}\bar{\mathbf{H}}_{qM})^{-1}\bar{\mathbf{H}}_{qM}^{H}. \tag{29}$$

Therefore, it attempts to remove the inter channel interference with the so-called pseudo inverse of the channel matrix [25]. However, ZF receivers are characterized by a main drawback, i.e. noise enhancement when the entries of the channel matrix have low values (around zero). The inversion enhances the noise variance, introducing some errors in the estimation of the transmitted symbols. As a consequence, any noise added after the channel gets boosted by a large factor and destroys the overall SNR. Furthermore, the channel may have zeroes in its frequency response that cannot be inverted at all. Some post processing SNR operation is usually adopted to match the noise variance [25];

- **MMSE Receiver** is the most balanced among the linear equalizers that gives a trade-off between noise enhancement and ISI. The expression of the demodulation matrix is

$$\mathbf{C}_{qM,\mathrm{MMSE}} = (\bar{\mathbf{H}}_{qM}^{H}\bar{\mathbf{H}}_{qM} + N_0\mathbf{I}_M)^{-1}\bar{\mathbf{H}}_{qM}^{H}, \tag{30}$$

where N_0 is the variance of the noise and $\mathbf{I}_M$ is an $M \times M$ identity matrix. The MMSE equalizer works as ZF at high SNR while it provides better performance in terms of distortion mitigation from lower to intermediate SNR values. Its main characteristic is that of not amplifying the noise when deep nulls appear in the frequency response of the channel.

Hence, to summarize, the linear ZF detector is preferable in interference-dominated scenarios, the linear MF detector is preferable in noise-dominated scenarios, while the linear MMSE detector is preferable in scenarios where the noise and the interference have a comparable level[25].

Singular Value Decomposition (SVD) is another linear processing technique can be used when the channel matrix is also known at the transmitter side as well as at the receiver. This method is based on the computation of the SVD

of the channel matrix

$$\mathbf{H}_{qM} = \bar{\mathbf{U}}_{qM}\bar{\mathbf{I}}_{qM}\bar{\mathbf{V}}_{qM} \tag{31}$$

where $\bar{\mathbf{U}}_{qM}$ and $\bar{\mathbf{V}}_{qM}$ are orthonormal matrices and $\mathbf{I}_{qM}$ is a diagonal matrix. A pre-processing operation is done on the M-symbols transmitted on the qth sub-carrier, as follow:

$$\mathbf{X}_{q_{pre-pro}} = \bar{\mathbf{V}}_{qM}\mathbf{X}_q \tag{32}$$

Then, the received signal is linearly transformed to get an estimation of the transmitted symbols:

$$\bar{\mathbf{X}}_q = \bar{\mathbf{U}}_{qM}^H\mathbf{Y}_q \tag{33}$$

Therefore, the elements of the received signal are decoupled and may be detected individually. This technique allows to split the computation cost of the processing operations, but the channel state information (CSI) is needed both at the transmitter and at the receiver [25]. The transmission becomes equivalent to that over a set of parallel channels, for each of which a separate and independent detection of transmitted symbols can be implemented.

6. Simulation Results

The performance of the proposed linear and non-linear designs is evaluated by means of Monte Carlo simulations. Now on, the metric used to evaluate the reliability of the proposed GFDM communication system is the Symbol Error Rate (SER) versus SNR, which is defined as the ratio between the energy of the transmitted symbol E_s and the power spectral density of the noise N_0. The SER is used as performance metric in this section, since the aim of the paper is to show the impact of the interference modelling on detection of symbols and how the different equalizers behave. Figures 4 and 5 report the performance of a GFDM signal transmission over a frequency selective channel modeled as (11) with length $L = 9$ for $K = 32$ and $M = 5$. Different results are reported for the

detection schemes described in Sec. 5. As mentioned before, at low SNR values all the equalizers have the same trend, since the errors due to the presence of the noise and fading are more

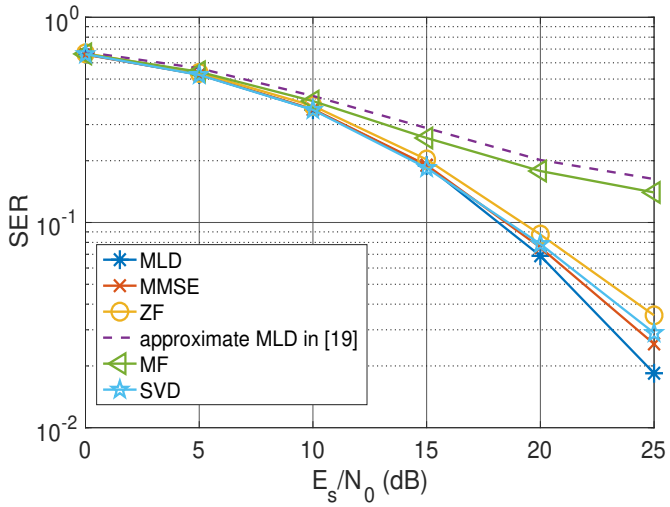

Figure 4: SER vs E_s/N_0 for the DGT-based GFDM with Dirichlet pulse shaping filter and different types of per sub-carrier receivers, in case of 8-PSK transmission over frequency selective Rayleigh fading channel with L=9 paths and with K=32 and M=5.

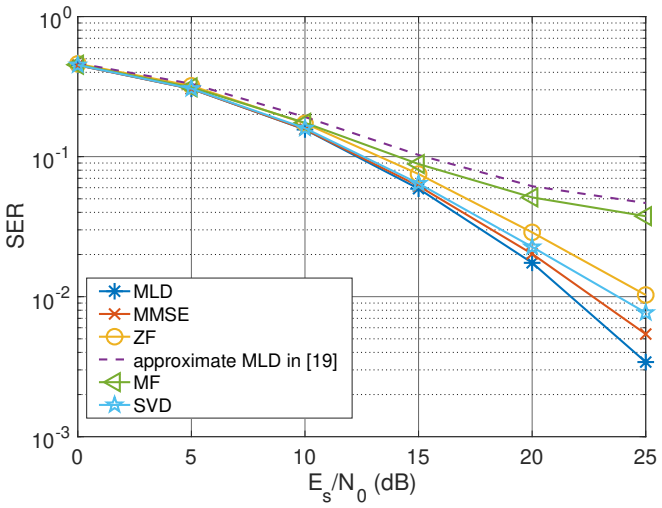

Figure 5: SER vs E_s/N_0 for the DGT-based GFDM with Dirichlet pulse shaping filter and different types of per sub-carrier receivers, in case of QPSK transmission over frequency selective Rayleigh fading channel with L=9 paths and with K=32 and M=5.

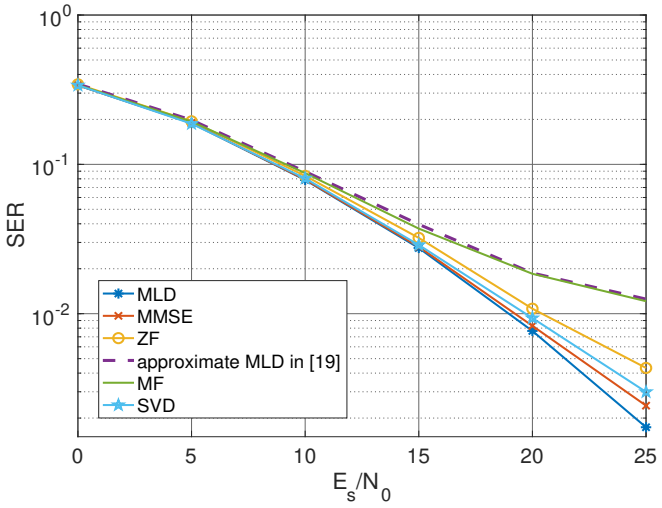

Figure 6: SER vs E_s/N_0 for the DGT-based GFDM with Dirichlet pulse shaping filter and different types of per sub-carrier receivers, in case of QPSK transmission over frequency selective Rayleigh fading channel with L=9 paths and with K=64 and M=7.

significant than those due to the effect of ISSI. When the SNR increases, both the MF and the method proposed in [19] show a performance floor with a degradation phenomenon. This is due to the fact that the presence of ISSI is not considered in a proper way, which clearly highlights the detrimental effect of neglecting it. As expected, the optimal receiver, in term of error rate, is the one based on MLD of the transmitted symbols on which comes at the cost of higher complexity. Instead, the MMSE allows a good trade-off between complexity and reliability. If also the transmitter knows the channel matrix of the qth sub-carrier $\bar{\mathbf{H}}_{qM}$ a pre-coding operation can be done based on SVD to obtain a performance gain with respect to the ZF equalizer, being the noise enhancement problem of this latter not present. However, this requires the knowledge of the channel also at the transmitting side of the link, which often is not the case.

By increasing the number of sub-carriers K the effect of the fading channel is more incisive and, therefore, the errors due to ISSI and the difference in performance is more evident for higher values of SNR, as can be seen in Fig. 6.

On the other hand interesting results come up when the value of M is changed. In fact, as shown in Figs. 7-10, the performance is almost the same for all the considered values of M, except for the limit case of $M = 1$, i.e. OFDM. It can be observed that at values of SNR greater than 20 dB there is gain for $M = 3, 5, 7$ compared to $M = 1$, which is due to a slightly change in the slope of the curve. The change in the slope is more evident for MLD and linear MMSE detection since, in comparison to other detectors, it starts at lower values of SNR. This can be observed in Figs. 7-9, where the results obtained for MLD in Figs. 7 and 8 and linear MMSE in Fig. 9 are reported for the same channel lengths and values of M considered for the linear ZF case in Fig. 10. It can be seen that for $M > 1$ at high SNR values an improvement in performance is achieved. This can be justified through a higher diversity gain factor that increases proportionally to M.

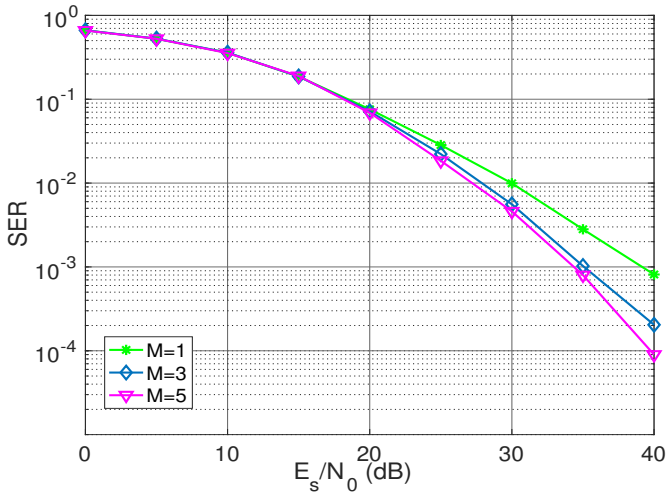

Figure 7: SER vs E_s/N_0 for the DGT-based GFDM with Dirichlet pulse shaping filter and per sub-carrier MLD, in case of 8-PSK transmission over frequency selective Rayleigh fading channel with L=9 paths and K =32 for different values of M=1, 3, 5. A performance gain is shown at higher SNR for $M > 1$.

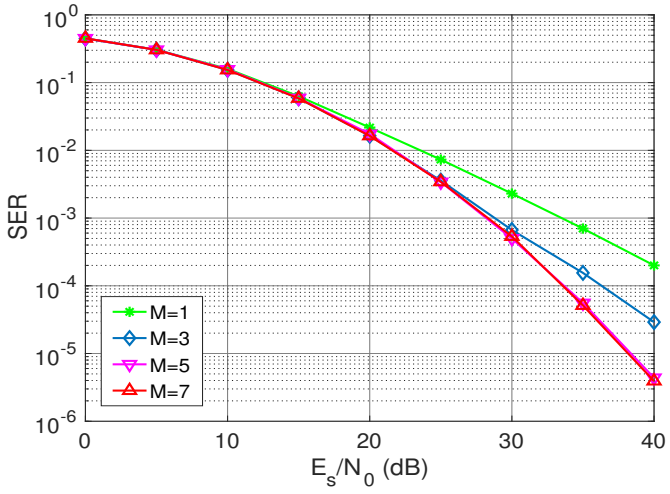

Figure 8: SER vs E_s/N_0 for the DGT-based GFDM with Dirichlet pulse shaping filter and per sub-carrier MLD, in case of QPSK transmission over frequency selective Rayleigh fading channel with L=9 paths and K =32 for different values of M=1, 3, 5, 7. A performance gain is shown at higher SNR for $M > 1$.

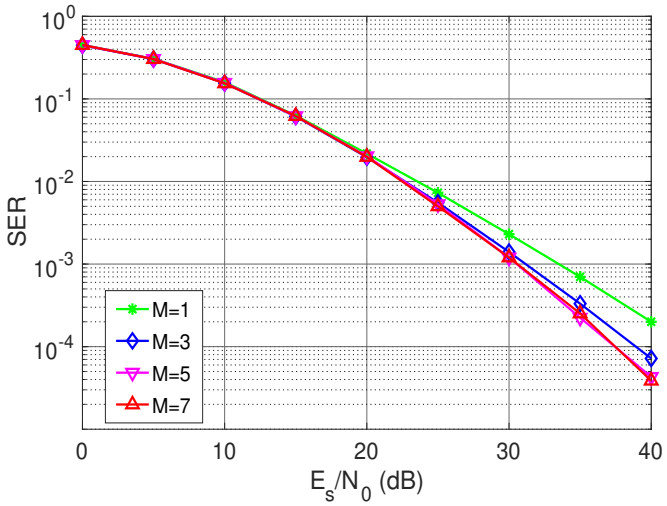

Figure 9: SER vs E_s/N_0 for the DGT-based GFDM with Dirichlet pulse shaping filter and per sub-carrier linear MMSE, in case of QPSK transmission over frequency selective Rayleigh fading channel with L=9 paths and K=32 for different values of M=1, 3, 5, 7. A performance gain is shown at higher SNR for $M > 1$.

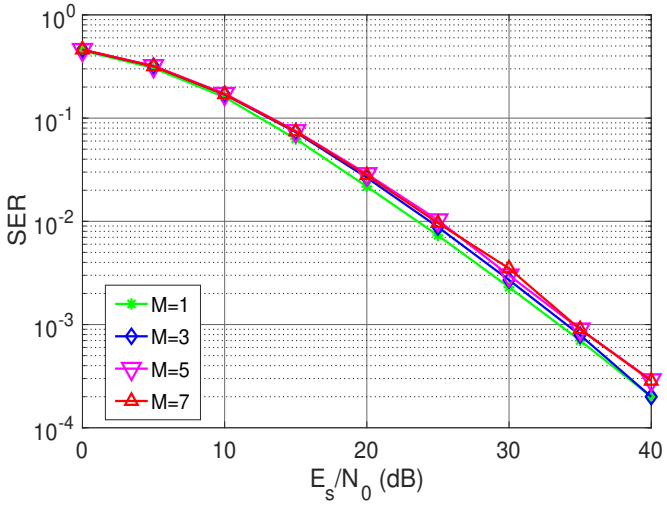

Figure 10: SER vs E_s/N_0 for the DGT-based GFDM with Dirichlet pulse shaping filter and per sub-carrier linear ZF, in case of QPSK transmission over frequency selective Rayleigh fading channel with L=9 paths and K=32 for different values of M=1, 3, 5, 7.

In fact, (25) is a circulant matrix, meaning that each row is a shifted version of the first one. This leads to a recursive description of the channel gain on the qth sub-carrier and the relative channel weights for the different sub-symbols transmitted on it. Thus, the detector is able to combine this information, as demonstrated in [27], allowing for a better detection of all the sub-symbols transmitted on the considered sub-carrier. Obviously, this does not happen for M=1 since (25) reduces to a Single Input Single Output (SISO) channel. A saturation effect is observed for $M = 5, 7$.

For channels characterized by a smaller number of taps L, a performance improvement is observed. This is related to the fact that the lower is L and the lower is the delay spread so, the higher the coherence bandwidth B_c. If B_c is greater than the signal bandwidth, the channel does not introduce any type of distortion on signal frequency response and also the ISSI reduces. This aspect can be observed in Fig. 11, where the performance trend of a GFDM signal, with a fixed number of sub-carriers K and symbols per sub-carrier M, are reported over a $L = 2, 5, 9$ paths channel.

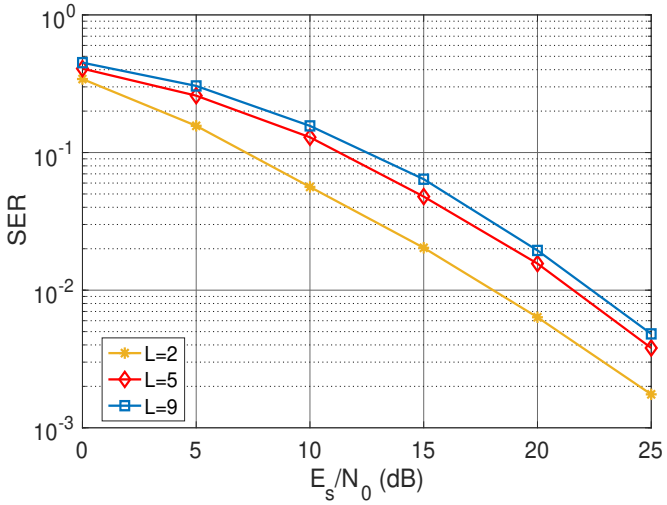

Figure 11: SER vs E_s/N_0 for the DGT-based GFDM with Dirichlet pulse shaping filter and per sub-carrier MLD, in case of QPSK transmission over frequency selective Rayleigh fading channels with different number of paths L=2, 5, 9 and with K=32 and M=5.

7. Complexity Analysis

In this section the implementation complexity of the operations performed at the receiver is evaluated by taking into account the number of complex multiplications. The main contributions to the computational cost are:

- $MK \times M$ multiplications to calculate $\gamma^*_{q,m}[n]y(n)$;
- MK-point FFT for computing $Y_q(m)$, as given in the first row of (14).
- implementation of the different detection algorithms, as given in Table 2.

The first two are common to all the detection methods and, therefore, differences are only in the implementation cost of the different detection methods. Figure 12 reports graphically the trend of the equalizers complexity for different values of M. The MLD and the approach proposed in [19] are the most expensive ones since their complexity is proportional to $\mathcal{X}^m$. From the presented results it appears that linear MMSE and linear ZF provide the best trade-off between computational cost and performance. In the same way, the method based on the SVD is not so computational expensive but, as already stated, the channel matrix has to be known also at the transmitter side.

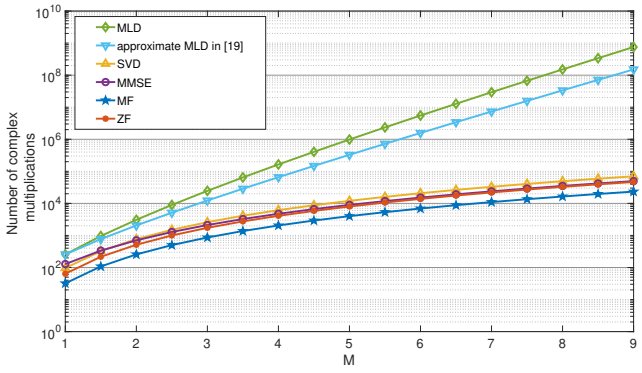

Figure 12: Numbers of complex multiplication vs. number of sub symbols per subcarrier M, for the different equalizer procedures and K=32.

multiplication between two $M \times M$ matrices	$\mathrm{O}(M^3)$
summation or subtraction between two $M \times M$ matrixes	$\mathrm{O}(M^2)$
$M \times M$ matrix inversion	$\mathrm{O}(M^3)$
$M \times M$ matrix svd	$\mathrm{O}(M^3)$

Table 1: General costs for matrix operations

8. Conclusion

In this work a mathematical framework for the description of the transmission and reception of DGT based GFDM signal over a frequency selective channel has been introduced. The description of the concept of Inter Sub Symbols Interference (ISSI) was modeled in closed form.

Detection scheme	operations done	cost
MF [18]	matrix multiplication	KM^3
ZF [18]	matrix multiplication + pseudo-inversion	$2KM^3$
SVD	svd calculation + 2× matrix multiplication	$3KM^3$
MMSE [18]	ZF operations + multiplication $N_0\mathbf{I}_M$ +matrix summation	$K(2M^3+M^2+M)$
MLD	exhaustive research and matrix $M \times M$ and vector $M \times 1$ multiplication + vector $M \times 1$ subtraction + squared modulul	$K\mathcal{X}^M(M^2+M)$
approximate MLD in [19]	exhaustive research x (diagonal matrix $M \times M$ and vector $M \times 1$ multiplication + vector $M \times 1$ subtraction + squared modulus)	$2KM\mathcal{X}^M$

Table 2: Cost for the equalization schemes

Thanks to the novel and suggested ISSI modelling, different types of linear and non-linear detection methods were designed and considered. Each one is characterized by pro and cons that were analyzed, investigated, and described in depth. Hence, it is possible to choose the most appropriate receiver method according to the desired degree of complexity and performance. Monte Carlo simulations were used to measure the error rate performance of the considered linear and non-linear receivers over frequency and non-frequency selective channels. Numerical results show that the design allows for improvement of performance compared to other methods proposed in the literature. These latter exhibit an error floor at high SNR since they are not able to take into account ISSI.

References

[1] E. Calvanese- Strinati, S. Barbarossa, J.-L. Gonzalez-Jimenez, L. Maret, D. Ktenas, N. Cassiau, and C. Dehos, "6G: The Next Frontier", in arXiv preprint arXiv:1901.03239, 2019

[2] B. Miscopein, J. Doré, E- Strinati, D. Kténas, S. Barbarossa, "Air Interface Challenges and Solutions for future 6G Networks", 2019, in CEA-01986524v2

[3] X. Zhang *et al.*, "On the waveform for 5G," *IEEE Commun. Mag.*, vol. 54, no. 11, pp. 74–80, Nov. 2016.

[4] Y. Cai, Z. Qin, F. Cui, G. Y. Li and J. A. McCann, "Modulation and multiple access for 5G networks," *IEEE Comm. Sur. Tut.*, vol. 20, no. 1, pp. 629–646, Mar. 2018.

[5] T. Taleb and A. Kunz, "Machine type communications in 3GPP networks: potential, challenges, and solutions," *IEEE Comm. Mag.*, vol. 50, no. 3, pp. 178–184, March. 2012.

[6] A. A. Zaidi *et al.*, "Waveform and numerology to support 5G services and requirements," *IEEE Commun. Mag.*, vol. 54, pp. 90–98, Nov. 2016.

[7] G. Wunder, *et al.*, "5GNOW: non-orthogonal, asynchronous waveforms for future mobile applications," *IEEE Commun. Mag.*, vol. 52, no. 2, pp. 97–105, Feb. 2014.

[8] P. Schulz, *et al.*, "Latency critical iot applications in 5G: perspective on the design of radio interface and network architecture," *IEEE Commun. Mag.*, vol. 55, no. 2, pp. 70–78, Feb. 2017.

[9] C. J. Zhang *et al.*, "New waveforms for 5G networks," *IEEE Commun. Mag.*, vol. 54, no. 11, pp. 64–65, Nov. 2016.

[10] N. Michailow *et al.*, "Generalized frequency division multiplexing for 5th generation cellular networks," *IEEE Trans. Comm.*, vol. 62, no. 9, pp. 3045–306, Sept. 2014.

[11] F. Schaich and T. Wild, "Waveform contenders for 5G: OFDM vs. FBMC vs. UFMC," in Proc. of *ISCCSP*, pp. 457-460, May 2014.

[12] A. Kumar and M. Magarini, "Improved Nyquist pulse shaping filters for generalized frequency division multiplexing," in Proc. of *LATINCOM*, pp. 1-7, Nov. 2016.

[13] H. Elayan, O. Amin, R. M. Shubair, M.-S. Alouini, "Terahertz communication: the opportunities of wireless technology beyond 5G," in Proc. of *IEEE CommNet*, 2018, pp. 1–5.

[14] S. Mumtaz, J. M. Jornet, J. Aulin, W. H. Gerstacker, X. Dong, "Terahertz communication for vehicular networks," *IEEE Transactions on Vehicular Technology*, vol. 66, no. 7, pp. 5617-5625, July 2017.

[15] N. Michailow and G. Fettweis, "Low peak-to-average power ratio for next generation cellular systems with generalized frequency division multiplexing," in Proc. of *IEEE International Symposium on Intelligent Signal Processing and Communication Systems*, 2013, pp. 651–655.

[16] E. Öztürk. E. Basar, H. A. Çırpan, "Spatial modulation GFDM: a low complexity MIMO-GFDM system for 5G wireless networks", in Proc. of *IEEE BlackSeaCom*, 2016, pp. 1–5.

[17] M. Sameen, et al., "Comparison of GFDM and OFDM with respect of SER, PSD and PAPR", IJMCA, Vol. 4, No. 6, Nov-Dec

[18] M. Matthé, L. L. Mendes, and G. Fettweis, "Generalized frequency division multiplexing in a Gabor transform setting," *IEEE Commun. Lett.*, vol. 18, pp. 1379–1382, Aug. 2014.

[19] P. Wei, X. G. Xia, Y. Xiao, S. Li, "Fast DGT-based receivers for GFDM in broadband channels," *IEEE Trans. Commun.*, vol. 64, pp. 4331–4345, Oct. 2016.

[20] A. Kumar and M. Magarini, "On the Modeling of Inter-Sub-Symbol Interference in GFDM Transmission," in IEEE Communications Letters, vol. 23, no. 10, pp. 1730-1734, Oct. 2019.

[21] H.G. Feichtinger, T. Strohmer (Eds.), "Gabor Analysis and Algorithms: Theory and Applications", Birkhäuser, Boston (1998)

[22] A. B. Üçüncü and A. Ö. Yılmaz, "Out-of-band radiation comparison of GFDM, WCP-COQAM and OFDM at equal spectral efficiency," *arXiv preprint arXiv:1510.01201*, 2015.

[23] M. K. Simon and M.-S. Alouini, *Digital Communication over Fading Channels, 2nd ed.* New York: Wiley, 2005.

[24] H. Artes, D. Seethaler, F. Hlawatsch, "Efficient detection algorithms for MIMO channels: a geometrical approach to approximate ML detection," *IEEE Trans. Sig. Proc.*, vol. 51, no. 11, pp. 2808–2820, Nov 2003.

[25] S. Yang and L. Hanzo, "Fifty Years of MIMO Detection: The Road to Large-Scale MIMOs," in IEEE Communications Surveys and Tutorials, vol. 17, no. 4, pp. 1941-1988, Fourthquarter 2015

[26] A. H. Mehana, A. Nosratinia, "Diversity of MMSE MIMO receivers," *IEEE Transactions on information theory*, vol. 58, no. 11, pp. 6788–6805, Nov. 2012.

[27] Xu Zhu and R. D. Murch, "Performance analysis of maximum likelihood detection in a MIMO antenna system," in IEEE Trans. on Commun., vol. 50, pp. 187-191, Feb. 2002.

[28] Y. Hame, et al, "Performance Analysis of Matched Filter Detector for MIMO Systems in Rayleigh Fading Channels", GLOBECOM 2017 - 2017 IEEE Global Communications Conference, Singapore, 2017, Pp. 1-6